Tamsir et al. Beni-Suef Univ J Basic Appl Sci (2023) 12:95
https://doi.org/10.1186/s43088-023-00434-0

Beni-Suef University Journal of Basic and Applied Sciences

RESEARCH

Open Access

A hybrid B-spline collocation technique for the Caputo time fractional nonlinear Burgers' equation

Mohammad Tamsir[1], Deependra Nigam[2], Neeraj Dhiman[3*] and Anand Chauhan[2]

Abstract

Background This study proposes an efficient and stable technique based on new hybrid B-spline (HB-spline) functions for the numerical treatment of the Caputo time fractional nonlinear Burgers' (TFNB) equation. The time derivative is discretized using the definition of the Caputo derivative, whereas HB-spline functions are used to discretize the spatial derivatives. The Rubin–Graves technique is used to linearize the nonlinear terms.

Results The performance and efficacy of the established method are tested using three examples. The graphical results represent the smoothness between numerical and exact solutions. The absolute errors are very low as 10^{-4} and 10^{-5}. The convergence rate shows that the proposed method is second-order accurate in space.

Conclusions The proposed method provides better results than the methods available in the literature. The method yields highly accurate results and can handle large-scale problems, which is the novelty of the present work.

Keywords Caputo TFNB equation, HB-spline basis functions, Stability analysis, Convergence rate

1 Background

The time fractional partial differential equations have grown more attention outstanding to several real-life applications in electrical network systems, signal processing, optics, mathematical biology, financial evaluation and prediction, material science, electromagnetic control theory, multidimensional fluid flow, acoustics, pre-predator modeling in biological systems, and many more [2, 3, 5–8]. The delayed time fractional predator–prey model with feedback control has been studied by Hopf bifurcation [10, 11]. For better accuracy in real-life models, the applications of fractional models are growing and indicate significant requirements for better fractional mathematical models. Radial basis functions and Laplace transformation are used for the approximation of fractional anomalous sub-diffusion equation [12]. This process's advantage is handling many matrix data efficiently and accurately. Padder et al. [32] recently performed a dynamical analysis of a generalized tumor model via the Caputo fractional-order derivative. The Caputo fractional-order derivative is being employed to model biological systems, including tumor growth. Tumor growth models are extensively used in biomedical research to understand tumor development dynamics and evaluate potential treatments.

Various analytical approaches are accessible for the numerical simulation of fractional partial differential equations. Typically, these types of equations are complicated to handle analytically. Thus, numerical approaches play a massive role in numerical approximations. For example, existing collocation methods based on Jacobi–Gauss–Lobatto have been generalized in [15]. Chebyshev polynomials in spectral collocation

*Correspondence:
Neeraj Dhiman
ndhiman@gehu.ac.in
[1] Department of Mathematics, Jazan University, 45142 Jazan, Saudi Arabia
[2] Department of Mathematics, Graphic Era Deemed to be University, Dehradun 248002, India
[3] Department of Mathematics, Graphic Era Hill University, Dehradun 248002, India

have been used to compute the space-fractional KdV–Burgers' equation [16], where Caputo–Fabrizio treats the space-fractional derivative. The spectral Pell collocation technique for approximating the TFNB equation has been used in [17]. The authors of [18] used the Hermite cubic spline collocation technique for the computational approximation of Helmholtz and Burgers' equations. The authors of [19, 21, 35, 36] used the quadratic B-spline Galerkin (QBSG) method, balanced space–time Chebyshev spectral collocation method, finite element method based on the cubic B-spline collocation method, and trigonometric tension B-spline collocation method, respectively, for TFNB equations. A practical and accurate technique based on the shifted Gegenbauer polynomials has been presented in [24] to simulate the multidimensional space-fractional coupled Burgers' equations. The residual power series method was utilized for time fractional BBM Burgers by Zhang et al. [25] and found that it is in good arrangement with the exact solution. Different fractional differential operators are applied for the analytical result of the TFNB equation [26]. Analytical approaches for approximating the fractional Burger's equation are presented in [27, 28].

A cubic B-spline FEM is applied in [13] to estimate time fractional Fisher's as well as Burgers' equations, while the authors of [14] used a collocation method based on Fibonacci polynomial and finite difference method to solve coupled fractional Burgers' equations. The authors of [22, 23] developed computational techniques based on cubic trigonometric B-splines (CTBS) and cubic parametric splines (CPS) to approximate the TFNB equation. Recently, Shafiq et al. [9] represented a numerical technique based on cubic B-spline (CB-spline) functions for the TFNB equation with the Atangana–Baleanu derivative. In addition, the authors of [1] discussed a numerical scheme for the Riemann–Liouville fractional integral. Further, they suggested two numerical schemes for the Caputo–Fabrizio and the Atangana–Baleanu integral operators. They analyzed that the Riemann–Liouville fractional integral yields smaller errors and an intense significant experimental convergence order in most functions, especially when the fractional order $\alpha \to 0$. A new adaptive numerical technique is proposed in [2] to solve nonlinear, singular, and stiff initial value problems frequently challenged in real life.

The arrangement of the paper is structured as follows. The discretization of the TFNB equation is given in Sect. 2. In Sect. 3, the von Neumann stability is discussed. Section 4 presents numerical results, while Sect. 5 presents its discussion. Finally, Sect. 6 highlights the conclusions.

2 Methods

2.1 Problem formulation

We establish a new hybrid B-spline collocation technique for following the Caputo TFNB equation.

$$\frac{\partial^\alpha v}{\partial t^\alpha} + v\frac{\partial v}{\partial x} - \hat{\nu}\frac{\partial^2 v}{\partial x^2} = f(x,t),\ a \le x \le b,\ 0 < \alpha < 1, \tag{1}$$

Along with

$$v(x,0) = \phi(x), \tag{2}$$

$$v(a,t) = \psi_1(t),\ v(b,t) = \psi_2(t), \tag{3}$$

where the $\frac{\partial^\alpha v}{\partial t^\alpha}$ denotes the Caputo time fractional derivative as follows:

$$\frac{\partial^\alpha v}{\partial t^\alpha} = \frac{1}{\Gamma(1-\alpha)}\int_0^t (t-\varsigma)^{-\alpha}\frac{\partial v(x,\varsigma)}{\partial \varsigma}d\varsigma,\ 0 < \alpha < 1. \tag{4}$$

Now, let us specify the definitions of Caputo fractional integral and derivatives.

Definition 2.1 The Caputo integral of the function $g(t) \in \mathbb{R}$ of order $\alpha \ge 0$ is defined as follows:

$${}^{c}J^{\alpha}_{0,t}g(t) = \frac{1}{\Gamma(\alpha)}\int_0^t (t-\chi)^{\alpha-1}g(\chi)d\chi,\ \alpha > 0,\ t > 0.$$

Definition 2.2 The Caputo derivative of $g(t) \in \mathbb{R}$ is defined as follows:

$${}^{c}D^{\alpha}_{0,t}g(t) = \frac{1}{\Gamma\left(\hat{l}-\alpha\right)}\int_0^t (t-\chi)^{\hat{l}-\alpha-1}g^{\left(\hat{l}\right)}(\chi)d\chi,\ t > 0,\ \hat{l}-1 < \alpha < \hat{l} \in \mathbb{Z}^+.$$

2.2 Discretization of the problem

This part performs the procedure to discretize the Caputo TFNB equation using the cubic HB-spline collocation technique.

2.2.1 Caputo time fractional derivative

First, we do a uniform partition in [0, T] with length $\Delta t = \frac{T}{N}$. Here N is the number of partitions in the time mesh. Now, the discretization of fractional derivatives $\frac{\partial^\alpha v}{\partial t^\alpha}$ for $0 < \alpha < 1$ at $t = t_{j+1}$ is given by L1 formula [20, 29, 30] as follows:

$$\frac{\partial^\alpha v_i^{j+1}}{\partial \tau^\alpha} = a_0 \sum_{k=0}^{j} P_k \left(v_i^{j-k+1} - v_i^{j-k} \right) + \hat{r}^{j+1},\ j = 0, 1, 2 \ldots N, \tag{5}$$

where $a_0 = \frac{\Delta t^{-\alpha}}{\lceil 2-\alpha}$, $p_j = (j+1)^{1-\alpha} - j^{1-\alpha}$, $j = 0, 1, 2....N$, and truncate error represented as $\hat{r}^{j+1}$ which is described by $\hat{r}^{j+1} \leq k_v \Delta t^{2-\alpha}$, where k_v is a constant only related to dependent variable v.

Lemma 2.1 The factor p_k, occurring in Eq. (5), satisfies the following properties:

$$\begin{cases} p_k > 0,\ k = 0, 1, ..., N, \\ 1 = p_0 > p_1 > p_2 > ... > p_N,\ p_N \to 0 \text{ as } N \to \infty, \end{cases}$$

Proof For proof of Lemma, see references [20, 29].

2.2.2 Spatial derivatives

Now, we use the HB-spline collocation technique for discretizing the spatial derivatives. The domain [a, b] is partitioned uniformly with the space size $h = \Delta x = \frac{b-a}{M}$ by the knots $x_i = a + ih$, $i = 0, 1, \ldots M$, so that we possess $a = x_0 < x_1 < x_2 < \ldots < x_M = b$. Now, we specify the HB-spline functions $Hb_i(x)$ for $i = -1, 0, ..., M+1$ as follows:

$$Hb_i(x) = \frac{1}{h^3} \begin{cases} \sigma (x - x_{i-2})^3 + (1-\sigma) b_2 \left\{ -\frac{1}{\hat{p}} \left(\sinh \left((x_{i-2} - x)\hat{p} \right) \right) + (x_{i-2} - x) \right\},\ x \in [x_{i-2}, x_{i-1}), \\ \sigma \left\{ h^3 + 3h^2 (x - x_{i-1}) + 3h (x - x_{i-1})^2 - 3 (x - x_{i-1})^3 \right\} + \\ (1-\sigma) \{ a_1 + b_1 (x_i - x) + c_1 e^{\hat{p}(x_i - x)} + d_1 e^{\hat{p}(x - x_i)} \},\ x \in [x_{i-1}, x_i), \\ \sigma \left\{ h^3 + 3h^2 (x_{i+1} - x) + 3h (x_{i+1} - x)^2 - 3 (x_{i+1} - x)^3 \right\} + \\ (1-\sigma) \{ a_1 + b_1 (x - x_i) + c_1 e^{\hat{p}(x - x_i)} + d_1 e^{\hat{p}(x_i - x)} \},\ x \in [x_i, x_{i+1}), \\ \sigma (x_{i+2} - x)^3 + (1-\sigma) b_2 \left\{ -\frac{1}{p} \left(\sinh \left(\hat{p} (x - x_{i+2}) \right) \right) + (x - x_{i+2}) \right\},\ x \in [x_{i+1}, x_{i+2}), \\ 0,\ \text{otherwise}, \end{cases} \tag{6}$$

where

$$a_1 = \frac{\hat{p}h\hat{\varsigma}_1}{\hat{p}h\hat{\varsigma}_1 - \hat{\varsigma}_2},\ b_1 = \frac{\hat{p}}{2} \left(\frac{\hat{\varsigma}_1 (\hat{\varsigma}_1 - 1) + s^2}{(ph\hat{\varsigma}_1 - \hat{\varsigma}_2)(1 - \hat{\varsigma}_1)} \right),\ c_1 = \frac{1}{4} \left(\frac{e^{-\hat{p}h} (1 - \hat{\varsigma}_1) + \hat{\varsigma}_2 \left(e^{-\hat{p}h} - 1 \right)}{(\hat{p}h\hat{\varsigma}_1 - \hat{\varsigma}_2)(1 - \hat{\varsigma}_1)} \right)$$

$$d_1 = \frac{1}{4} \left(\frac{e^{\hat{p}h} (\hat{\varsigma}_1 - 1) + \hat{\varsigma}_2 \left(e^{\hat{p}h} - 1 \right)}{(\hat{p}h\hat{\varsigma}_1 - \hat{\varsigma}_2)(1 - \hat{\varsigma}_1)} \right),\ b_2 = \frac{\hat{p}}{2(\hat{p}h\hat{\varsigma}_1 - \hat{\varsigma}_2)},\ \hat{\varsigma}_1 = \cosh(\hat{p}h),\ \hat{\varsigma}_2 = \sinh(\hat{p}h).$$

Table 1 The values of $Hb_i(x)$ and its derivatives at the knots

	x_{i-2}	x_{i-1}	x_i	x_{i+1}	x_{i+2}
$Hb_i(x)$	0	τ_1	τ_2	τ_1	0
$Hb_i'(x)$	0	τ_3	0	$-\tau_3$	0
$Hb_i''(x)$	0	τ_4	$-2\tau_4$	τ_4	0

Where $\tau_1 = \sigma + (1-\sigma) \frac{\hat{\varsigma}_2 - \hat{p}h}{2(\hat{p}h\hat{\varsigma}_1 - \hat{\varsigma}_2)}$, $\tau_2 = 1 + 3\sigma$,

$\tau_3 = \frac{3\sigma}{h} + (1-\sigma) \frac{\hat{p}(\hat{\varsigma}_1 - 1)}{2(\hat{p}h\hat{\varsigma}_1 - \hat{\varsigma}_2)}$, $\tau_4 = \frac{6\sigma}{h^2} + (1-\sigma) \frac{\hat{p}^2 \hat{\varsigma}_2}{2(\hat{p}h\hat{\varsigma}_1 - \hat{\varsigma}_2)}$.

The HB-spline functions are obtained by using $Hb_i(x) = \sigma B_i(x) + (1-\sigma) EB_i(x)$, where $B_i(x)$ and $EB_i(x)$ are cubic B-spline basis functions [4, 31] and cubic exponential B-spline basis functions [3, 33, 34], and σ is a hybrid parameter. The term $\hat{p}$ is a free parameter which acquires various forms of cubic exponential B-spline basis functions. The HB-spline functions are piecewise basis functions with non-negativity, C^2 continuity, unity partition property, and form a basis in $[a, b]$. The values of $Hb_i(x)$, $Hb_i'(x)$, and $Hb_i''(x)$ are presented in Table 1.

We define the approximate solution as

$$u(x, t_j) \approx \sum_{i=-1}^{M+1} Hb_i(x) C_i(t_j), \tag{7}$$

where $C_i(t_j)$ is unknown quantities.

The variation of the $v(x, t_j)$ is stated as follows:

$$v(x,t_j) = \sum_{k=i-1}^{i+1} Hb_k(x)C_k(t_j). \tag{8}$$

Using above equation, we get the approximate values of v, v_x, and v_{xx} as

$$v_i^n = \tau_1 C_{i-1}^j + \tau_2 C_i^j + \tau_1 C_{i+1}^j, \tag{9}$$

$$(v_x)_i^j = -\tau_3 C_{i-1}^j + \tau_3 C_{i+1}^j, \tag{10}$$

and

$$(v_{xx})_i^j = \tau_4 (C_{i-1}^j - 2C_i^j + C_{i+1}^j). \tag{11}$$

At $t = t_{j+1}$, using Eq. (5) for the time fractional derivative, the problem (1) is discretized as follows:

$$a_0 \sum_{k=0}^{j} p_k \left(v_i^{j-k+1} - v_i^{j-k} \right) + v_i^{j+1}(v_x)_i^{j+1} - \hat{\nu}(v_{xx})_i^{j+1} = f_i^{j+1},\ i = 0,1,...,M,\ j = 0,1,...,N. \tag{12}$$

For linearizing the nonlinear term, we use the Rubin–Graves technique as follows:

$$(vv_x)_i^{j+1} = v_i^j (v_x)_i^{j+1} + v_i^{j+1}(v_x)_i^j - v_i^j (v_x)_i^j \tag{13}$$

By Eqs. (12) and (13), we have

$$a_0 \sum_{k=0}^{j} p_k \left(v_i^{j-k+1} - v_i^{j-k} \right) + v_i^j (v_x)_i^{j+1} + v_i^{j+1}(v_x)_i^j - v_i^j (v_x)_i^j - \hat{\nu}(v_{xx})_i^{j+1} = f_i^{j+1}. \tag{14}$$

We can rewrite above equation as follows:

$$a_0 \left[v_i^{j+1} - \sum_{k=0}^{j-1} (p_k - p_{k+1}) v_i^{j-k} - p_j v_i^0 \right] + v_i^j (v_x)_i^{j+1} + v_i^{j+1}(v_x)_i^j - v_i^j (v_x)_i^j - \hat{\nu}(v_{xx})_i^{j+1} = f_i^{j+1}. \tag{15}$$

$$\Rightarrow$$

$$\left(a_0 + (v_x)_i^j \right) v_i^{j+1} + v_i^j (v_x)_i^{j+1} - \hat{\nu}(v_{xx})_i^{j+1} = a_0 \sum_{k=1}^{j-1} \left((p_k - p_{k+1}) v_i^{j-k} + p_j v_i^0 \right) + v_i^j (v_x)_i^j + f_i^{j+1},\ i = 0,1,...,M,\ j = 0,1,...,N. \tag{16}$$

Now, using Eqs. (9)–(10) in above equation, we get

$$A_i^j C_{i-1}^{j+1} + B_i^j C_i^{j+1} + D_i^j C_{i+1}^{j+1} = R_i^j \quad i = 1,2,\ldots,M+1, j = 0,1,...,N, \tag{17}$$

where

$$A_i^j = \left(a_0 + (v_x)_i^j \right) \tau_1 - v_i^j \tau_3 - \hat{\nu}\tau_4,\ B_i^j = \left(a_0 + (v_x)_i^j \right) \tau_2 + 2\hat{\nu}\tau_4,\ D_i^j = \left(a_0 + (v_x)_i^j \right) \tau_1 + v_i^j \tau_3 - \hat{\nu}\tau_4,$$

$$R_i^j = a_0 \sum_{k=1}^{j-1} \left((p_k - p_{k+1}) v_i^{j-k} + p_j v_i^0 \right) + v_i^j (v_x)_i^j + f_i^{j+1}.$$

Equation (17) forms a system of linear equations with $M+1$ equations and $M+3$ unknows. For unique solution, we treat the boundary conditions $v(a,t) = \psi_1(t)$ and $v(b,t) = \psi_2(t)$ as

$$\left(\tau_1 C_{-1}^j + \tau_2 C_0^j + \tau_1 C_1^j \right) = \psi_1^j, \tag{18}$$

and

$$\left(\tau_1 C_{M-1}^j + \tau_2 C_M^j + \tau_1 C_{M+1}^j \right) = \psi_2^j, \tag{19}$$

Solving Eqs. (18) and (19), we get

$$C_{-1}^{j}=-\frac{\tau_2}{\tau_1}C_0^j-C_1^j+\frac{1}{\tau_1}\psi_1^j \text{ and } C_{M+1}^{j} = -C_{M-1}^{j}-\frac{\tau_2}{\tau_1}C_M^j+\frac{1}{\tau_1}\psi_2^j. \tag{20}$$

For $i=0$ and $i=M$, using (20) in (17), we have

$$\left(-\frac{\tau_2}{\tau_1}A_0^j+B_0^j\right)C_0^{j+1}+\left(-A_0^j+D_0^j\right)C_1^{j+1}=R_0^j-\frac{A_0^j}{\tau_1}\psi_1^{j+1}, \tag{21}$$

and

$$\left(A_M^j-D_M^j\right)C_{M-1}^{j+1}+\left(B_M^j-\frac{\tau_2}{\tau_1}D_M^j\right)C_M^{j+1}=R_M^j-\frac{D_M^j}{\tau_1}\psi_2^{j+1}. \tag{22}$$

Equations (21), (22), and (17) form a system of linear equations as follows:

$$\begin{bmatrix} -\frac{\tau_2}{\tau_1}A_0^j+B_0^j & -A_0^j+D_0^j & 0 & 0 & 0 & \cdots & 0 \\ A_0^j & B_0^j & C_0^j & 0 & 0 & \cdots & 0 \\ 0 & A_1^j & B_1^j & D_1^j & 0 & \cdots & 0 \\ \vdots & \ddots & \ddots & \ddots & \ddots & \vdots & \vdots \\ 0 & \cdots & 0 & A_{M-2}^j & B_{M-2}^j & D_{M-2}^j & 0 \\ 0 & \cdots & 0 & 0 & A_{M-1}^j & B_{M-1}^j & D_{M-1}^j \\ 0 & \cdots & 0 & 0 & 0 & A_M^j-D_M^j & B_M^j-\frac{\tau_2}{\tau_1}D_M^j \end{bmatrix}\begin{bmatrix} C_0^0 \\ C_1^0 \\ C_2^0 \\ \vdots \\ C_{M-2}^0 \\ C_{M-1}^0 \\ C_M^0 \end{bmatrix}=\begin{bmatrix} R_0^j-\frac{A_0^j}{\tau_1}\psi_1^{j+1} \\ R_1^j \\ R_2^j \\ \vdots \\ R_{M-2}^j \\ R_{M-1}^j \\ R_M^j-\frac{D_M^j}{\tau_1}\psi_2^{j+1} \end{bmatrix}.$$

To solve above system, we require to determine the initial vector $\left(C_0^0,C_1^0,...,C_{M-1}^0,C_M^0\right)$ from the initial condition which delivers $M+1$ equations with $M+3$ unknowns. To remove the C_{-1}^0 and C_{M+1}^0, we use the first derivative of the initial condition at the boundaries which gives:

$$C_{-1}^0=C_1^0-\frac{1}{\tau_3}(\phi_x)_0 \text{ and } C_{M+1}^0=C_{M-1}^0+\frac{1}{\tau_3}(\phi_x)_M, \tag{23}$$

Now using Eqs. (23) and (9), we have the following system of linear equations:

$$\begin{bmatrix} \tau_2 & 2\tau_1 & 0 & & & & \\ \tau_1 & \tau_2 & \tau_1 & & & & \\ 0 & \tau_1 & \tau_2 & \tau_1 & & & \\ & \ddots & \ddots & \ddots & & & \\ & & & \tau_1 & \tau_2 & \tau_1 & 0 \\ & & & & \tau_1 & \tau_2 & \tau_1 \\ & & & & 0 & 2\tau_1 & \tau_2 \end{bmatrix}\begin{bmatrix} C_0^0 \\ C_1^0 \\ C_2^0 \\ \vdots \\ C_{M-2}^0 \\ C_{M-1}^0 \\ C_M^0 \end{bmatrix}=\begin{bmatrix} \phi_0+\frac{\tau_1}{\tau_3}(\phi_x)_0 \\ \phi_1 \\ \phi_2 \\ \vdots \\ \phi_{M-2} \\ \phi_{M-1} \\ \phi_M-\frac{\tau_1}{\tau_3}(\phi_x)_M \end{bmatrix}.$$

3 Stability analysis

The stability analysis of the discretized system of the TFNB equation based on the von Neumann method [22, 36, 39] is established in this section. According to Duhamels' principle [40], it is assumed that the stability analysis of an inhomogeneous problem is an instantaneous consequence of the stability analysis for the subsequent homogeneous problem. So, for convenience and without loss of generality, we consider $f=0$, and we linearize the term vv_x by taking $v_x=\hat{k}_1$ as locally constants. Using above assumptions and some manipulation, Eq. (12) can be rewritten as follows:

$$\begin{aligned} &A^*C_{i-1}^{j+1}+B^*C_i^{j+1}+D^*C_{i+1}^{j+1} \\ &=a_0\sum_{k=0}^{j-1}\left(P_k-P_{k+1}\right)\left(\tau_1C_{i-1}^{j-k}+\tau_2C_i^{j-k}+\tau_1C_{i+1}^{j-k}\right) \\ &\quad -a_0p_j\left(\tau_1C_{i-1}^0+\tau_2C_i^0+\tau_1C_{i+1}^0\right) \\ &\quad -a_0p_j\left(\tau_1C_{i-1}^0+\tau_2C_i^0+\tau_1C_{i+1}^0\right), \\ &i=0,1,...,M, j=0,1,...,N, \end{aligned} \tag{24}$$

where

$$A^*=D^*=\left(a_0+\hat{k}_1\right)\tau_1-\hat{\nu}\tau_4,\ B^*=\left(a_0+\hat{k}_1\right)\tau_2+2\hat{k}_1\tau_4.$$

Now, we take a Fourier mode as $C_i^j=\delta^je^{\hat{i}i\mu h}$, where $\hat{i}=\sqrt{-1}$, δ is the time-dependent constraint. Applying it into above equation and simplifying it, we get

$$\left(2A^{*}\cos(\mu h)+B^{*}\right)\delta^{j+1}=\left(a_0\sum_{k=0}^{j-1}\left(P_k-P_{k+1}\right)\delta^{j-k}-a_0p_j\delta^0\right)(2\tau_1\cos(\mu h)+\tau_2). \tag{25}$$

$$\Rightarrow\left[\left(2(a_0+\hat{k}_1)\tau_1-2\hat{\nu}\tau_4\right)\cos(\mu h)+(a_0+\hat{k}_1)\tau_2+2\hat{\nu}\tau_4\right]\delta^{j+1}=\left(a_0\sum_{k=0}^{j-1}\left(P_k-P_{k+1}\right)\delta^{j-k}-a_0p_j\delta^0\right)(2\tau_1\cos(\mu h)+\tau_2). \tag{26}$$

Now, we define

$$\delta^j_{\max}=\max_{0\le i\le j}\left|\delta^j\right|. \tag{27}$$

Using in above equation, we get

$$\left[\left(2(a_0+\hat{k}_1)\tau_1-2\hat{\nu}\tau_4\right)\cos(\mu h)+(a_0+\hat{k}_1)\tau_2+2\hat{\nu}\tau_4\right]\delta^{j+1}=\left(a_0\sum_{k=0}^{j-1}\left(P_k-P_{k+1}\right)-a_0P_j\right)\delta^j_{\max}(2\tau_1\cos(\mu h)+\tau_2), \tag{28}$$

Simplifying it, we have

$$\delta^{j+1}=\frac{a_0(2\tau_1\cos(\mu h)+\tau_2)}{\left(2(a_0+\hat{k}_1)\tau_1-2\hat{\nu}\tau_4\right)\cos(\mu h)+(a_0+\hat{k}_1)\tau_2+2\hat{\nu}\tau_4}\delta^j_{\max}. \tag{29}$$

The discretized system of the TFNB equation is unconditionally stable when $|\delta|\le 1$ which is obvious from above equation. One can see the alternative proof in [22].

4 Results

This section considers examples of TFNB equation to test the performance and efficacy of the established procedure. The rate of convergence (ROC) is analyzed by:

$\mathrm{ROC}=\frac{\log\left(E^{h_1}/E^{h_2}\right)}{\log(h_1/h_2)}$, where E^{h_1} and E^{h_2} signify the errors with h_1 and h_2, respectively. The error analysis is done in terms of L_2, L_∞ and RMS errors, defined by:

$L_2=\left(\sum|U_j-u_j|^2\right)^{1/2}$; $L_\infty=\max|U_j-u_j|$; $\mathrm{RMS}=\left(\sum\frac{|U_j-u_j|^2}{n}\right)^{1/2}$.

Example 1 Consider the TFNB Eq. (1) for $f(x,t)=\frac{2t^{2-\alpha}e^x}{\lceil 3-\alpha}+t^4e^{2x}-\hat{\nu}t^2e^x$ with $\nu(x,t)=t^2e^x$ in [0,1].

We fix free parameter $\hat{p}=5$ for all computations of Example 1. First, we approximate it with $\sigma=0.5$, $\alpha=0.5$, $\Delta t=0.00025$, and $\hat{\nu}=1$ at $t=1$ for grids $M=10$, 20, 40, and 80. The numerical solutions are presented in Table 2, while Table 3 compares L_2 and L_∞ errors of the proposed method with those available in Ref. [19] with $\alpha=0.5$, $\Delta t=0.00025$, and $\hat{\nu}=1$ at $t=1$ for hybrid parameters $\sigma=0.1$, 0.5, 0.9, and grids $M=10$, 20, 40, and 80. Now, we solve this example with the parameters $\sigma=0.5$, $\alpha=0.5$, $M=80$, $\hat{\nu}=1$ at $t=1$ for different $\Delta t=0.002$, 0.001, 0.0005, and 0.00025. The numerical solutions are presented in Table 4, while Table 5 compares L_2 and L_∞ errors of the proposed method with those available in Ref. [19]. The comparison of the proposed method with QBSG method [19] together with the convergence rate of the proposed method is shown in Table 6 for $\alpha=0.5$, $\sigma=0.5$, $\Delta t=0.00025$, and $\hat{\nu}=1$ at $t=1$. It is obvious that the proposed method is second-order accurate in space variable. The L_2 and L_∞ error norms with $\Delta t=0.00025$ and $\hat{\nu}=1$ at $t=1$ for fractional order $\alpha=0.1$ with hybrid parameters $\sigma=0.1$, 0.5, and 0.9 are demonstrated in Table 7. Figures 1 and 2 show the comparison of the exact and numerical solutions graphically with $\sigma=0.5$, $\alpha=0.5$, $M=10$, $\Delta t=0.00025$, and $\hat{\nu}=1$ for different times. Figure 2 demonstrates the exact and numerical solutions along with absolute errors for $\sigma=0.5$, $\alpha=0.5$, $M=80$, $\Delta t=0.05$, and $\hat{\nu}=1$ at $t=0.5$, while Fig. 3 shows it for $\sigma=0.9$, $\alpha=0.1$, $M=80$, $\Delta t=0.05$, and $\hat{\nu}=1$ at $t=1$.

Example 2 Now, we consider the TFNB Eq. (1) with the following initial and boundary conditions

$$\nu(x,0)=0,\ 0\le x\le 1,$$

and

$$\nu(0,t)=t^2,\ \nu(1,t)=-t^2,\ t\ge 0.$$

The exact solution is $\nu(x,t)=t^2\cos(\pi x)$, and the function $f(x,t)$ is

$$f(x,t)=\left(\frac{2t^{2-\alpha}}{\lceil 3-\alpha}+\pi t^2\left(\hat{\nu}\pi-t^2\sin(\pi x)\right)\right)\cos(\pi x).$$

Table 2 The comparison of present and existing numerical solutions with exact solutions for $\alpha = 0.5$, $\sigma = 0.5$, $\Delta t = 0.00025$, and $\hat{\nu} = 1$ at $t = 1$

x	Present method $M = 10$	QBSG method [19] $M = 10$	Present method $M = 20$	QBSG method [19] $M = 20$	Present method $M = 40$	QBSG method [19] $M = 40$	Present method $M = 80$	QBSG method [19] $M = 80$	Exact
0.0	1.000000	1.000000	1.000000	1.000000	1.000000	1.000000	1.000000	1.000000	1.000000
0.1	1.105304	1.105440	1.105204	1.105287	1.105179	1.105216	1.105173	1.105197	1.105171
0.2	1.221651	1.222203	1.221465	1.221644	1.221418	1.221493	1.221407	1.221455	1.221403
0.3	1.350204	1.351078	1.349946	1.350217	1.349880	1.349992	1.349864	1.349935	1.349859
0.4	1.492247	1.493437	1.491908	1.492287	1.491851	1.491996	1.491831	1.491922	1.491825
0.5	1.649197	1.650663	1.648841	1.649270	1.648751	1.648922	1.648729	1.648838	1.648721
0.6	1.822618	1.824294	1.822244	1.822727	1.822150	1.822342	1.822127	1.822247	1.822119
0.7	2.014238	2.016049	2.013874	2.014378	2.013783	2.013979	2.013760	2.013882	2.013753
0.8	2.225958	2.227650	2.225645	2.226118	2.225567	2.225747	2.225547	2.225661	2.225541
0.9	2.459872	2.461512	2.459670	2.460020	2.459620	2.459745	2.459607	2.459680	2.459603
1.0	2.718282	2.718282	2.718282	2.718282	2.718282	2.718282	2.718282	2.718282	2.718282

Table 3 The L_2 and L_∞ errors with $\alpha = 0.5$, $\Delta t = 0.00025$, and $\hat{\nu} = 1$ at $t = 1$

M	L_2				$L_\infty L_\infty$			
	Present			QBSG method [19]	Present			QBSG method [19]
	$\sigma = 0.1$	$\sigma = 0.5$	$\sigma = 0.9$		$\sigma = 0.1$	$\sigma = 0.5$	$\sigma = 0.9$	
10	2.59e−04	6.34e−05	5.23e−06	1.6329e−03	3.42e−04	8.37e−05	6.90e−06	2.2967e−03
20	6.47e−05	1.59e−05	1.25e−06	4.4772e−04	8.59e−05	2.11e−05	1.66e−06	6.2502e−04
40	1.62e−05	4.00e−06	2.78e−07	1.6183e−04	2.15e−05	5.32e−06	3.67e−07	2.2735e−04
80	4.08e−06	1.03e−06	3.65e−08	1.1255e−05	5.42e−06	1.37e−06	4.72e−08	1.3312e−04

Table 4 The numerical solutions with $\sigma = 0.5$, $\alpha = 0.5$, $M = 80$, and $\hat{\nu} = 1$ at $t = 1$

x	Present method $\Delta t = 0.002$	QBSG method [19]	Present method $\Delta t = 0.001$	QBSG method [19]	Present method $\Delta t = 0.0005$	QBSG method [19]	Present method $\Delta t = 0.00025$	QBSG method [19]
0.0	1.000	1.000000	1.0000	1.000000	1.0000	1.000000	1.0000	1.000000
0.1	1.1052	1.105356	1.1052	1.105287	1.1052	1.105216	1.1052	1.105197
0.2	1.2214	1.221768	1.2214	1.221644	1.2214	1.221493	1.2214	1.221455
0.3	1.3499	1.350395	1.3499	1.350217	1.3499	1.349992	1.3499	1.349935
0.4	1.4918	1.492516	1.4918	1.492287	1.4918	1.491996	1.4918	1.491922
0.5	1.6487	1.649543	1.6487	1.649270	1.6487	1.648922	1.6487	1.648838
0.6	1.8221	1.823031	1.8221	1.822727	1.8221	1.822342	1.8221	1.822247
0.7	2.0138	2.014687	2.0138	2.014378	2.0138	2.013979	2.0138	2.013882
0.8	2.2255	2.226387	2.2255	2.226118	2.2255	2.225747	2.2255	2.225661
0.9	2.4596	2.460180	2.4596	2.460020	2.4596	2.459745	2.4596	2.459680
1.0	2.7183	2.718282	2.7183	2.718282	2.7183	2.718282	2.7183	2.718282

Table 5 The comparison of the proposed and existing methods in terms of L_2 and L_∞ with $\sigma=0.5$, $\alpha=0.5$, $M=80$, and $\hat{\nu}=1$ at $t=1$

	L_2		L_∞	
Δt	**Present**	**QBSG method [19]**	**Present**	**QBSG method [19]**
0.002	5.1434e−06	6.60788e−04	6.9801e−06	9.36619e−04
0.001	2.4367e−06	4.47720e−04	3.2687e−06	6.25018e−04
0.0005	1.4914e−06	1.61833e−04	1.9858e−06	2.27352e−04
0.00025	1.0339e−06	9.2624e−05	1.3741e−06	1.33125e−04

Table 8 shows the comparison of L_2 and L_∞ error norms for $\hat{p}=0.015$, $\sigma=0.5$, $\alpha=0.5$ $\Delta t=0.00025$, and $\hat{\nu}=1$ at $t=1$ for $M=10$, 20, 40, and 80. This table also establishes that the proposed method is second-order accurate in space variable. The error norms L_2 and L_∞ are calculated for $\hat{p}=0.015$, $\sigma=0.5$, $\alpha=0.5$ $M=80$, and $\hat{\nu}=1$ at $t=1$ for various time mesh sizes in Table 9. Now, Table 10 shows the comparison of error norms with $\sigma=0.5$, $M=80$, $\Delta t=0.00025$, and $\hat{\nu}=1$ at $t=1$ for various values of fractional orders $\alpha=0.1$, 0.25, 0.75, and

Table 6 The comparison of error norms together with the convergence rate of the present method for $\alpha=0.5$, $\sigma=0.5$, $\Delta t=0.00025$, and $\hat{\nu}=1$ at $t=1$

M	**Present method**				**Ref. [19]**	
	L_2	**ROC**	**L_∞**	**ROC**	**L_2**	**L_∞**
10	3.653495e−04	–	4.997399e−04	–	1.632995e−03	2.296683e−03
20	9.170910e−05	1.99	1.254263e−04	1.99	4.47720e−04	6.25018e−04
40	2.298575e−05	2.00	3.146194e−05	2.00	1.61833e−04	2.27352e−04
80	5.785360e−06	1.99	7.921316e−06	2.00	9.2624e−05	1.33125e−04

Table 7 The L_2 and L_∞ errors with $\alpha=0.1$, $\sigma=0.5$, $\Delta t=0.00025$, and $\hat{\nu}=1$ at $t=1$

M	**L_2**			**L_∞**		
	$\sigma=0.1$	**$\sigma=0.5$**	**$\sigma=0.9$**	**$\sigma=0.1$**	**$\sigma=0.5$**	**$\sigma=0.9$**
10	1.48405e−03	3.65349e−04	3.04107e−05	2.03008e−03	4.99739e−04	4.15952e−05
20	3.73408e−04	9.17091e−05	7.43431e−06	5.10699e−04	1.25426e−04	1.01667e−05
40	9.35362e−05	2.29857e−05	1.81275e−06	1.28024e−04	3.14619e−05	2.47969e−06
80	2.34308e−05	5.78536e−06	4.15071e−07	3.20782e−05	7.92132e−06	5.67154e−07

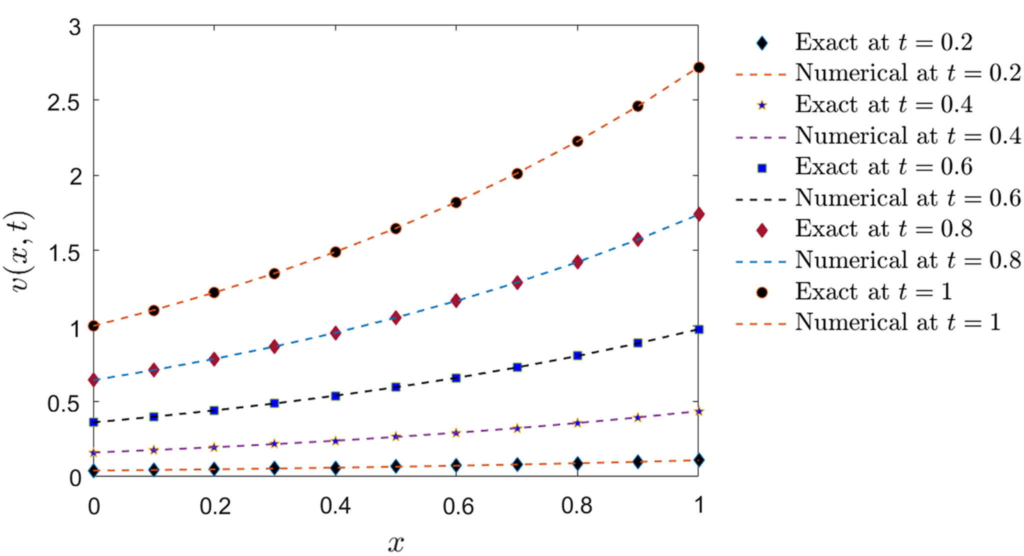

Fig. 1 The exact and approximate $v(x, t)$ with $\sigma=0.5$, $\alpha=0.5$, $\Delta t=0.00025$, $\hat{\nu}=1$, and $M=10$ at $t=0.2$, 0.4, 0.6, 0.8, and 1 for Example 1

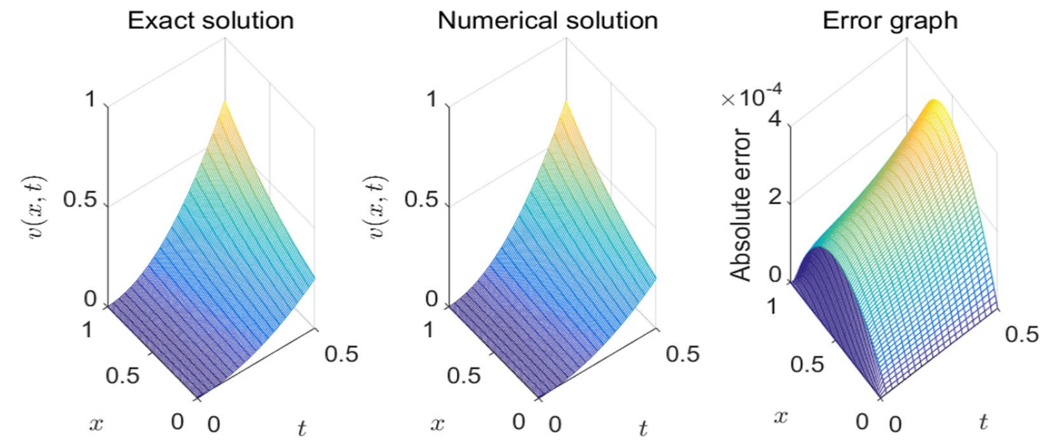

Fig. 2 The exact and approximate $v(x,t)$ along with abs. errors for $\sigma=0.5$, $\alpha=0.5$, $\Delta t=0.05$, v = 1, and $M=80$ at $t=0.5$ for Example 1

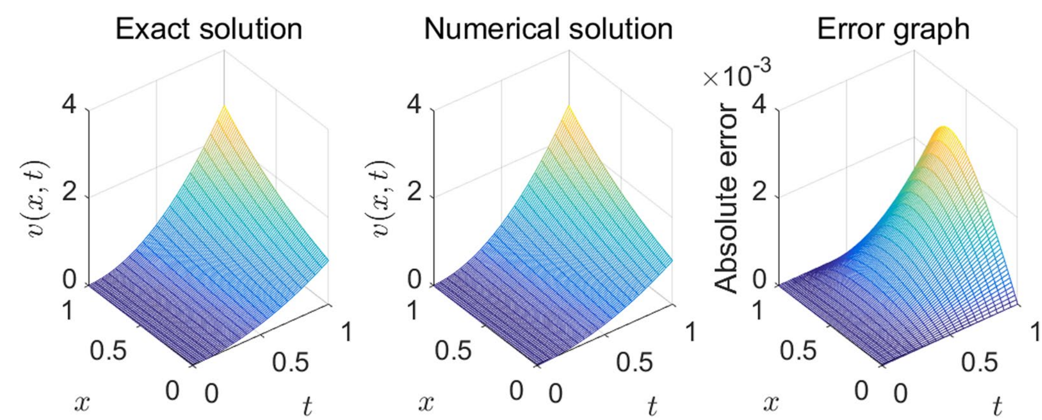

Fig. 3 The exact and approximate $v(x,t)$ along with abs. error for $\sigma=0.9$, $\alpha=0.1$, $\Delta t=0.05$, $\hat{\nu}=1$, and $M=80$ at $t=1$ for Example 1

1. Figure 4 exhibits that absolute error norms are very less ($\approx 10^{-5}$) for parameters $\alpha=0.5$, $\hat{p}=0.015$, $\sigma=0.5$, $M=80$, $\Delta t=0.0005$, and $\hat{\nu}=1$ at $t=0.2$, 0.4, 0.6, 0.8, and 1. Figure 5 shows the comparison of the exact and numerical solutions for $\alpha=0.5$, $\hat{p}=0.015$, $\sigma=0.5$, $\hat{\nu}=1$, $M=20$, and $\Delta t=0.001$ at various times, while Fig. 6 shows the surface behavior of the solutions for $\alpha=0.5$, $\hat{p}=0.015$, $\sigma=0.5$, $M=80$, $\Delta t=0.0005$, and $\hat{\nu}=1$.

Table 8 The comparison of error norms together with the convergence rate of the present method for $\alpha=0.5$, $\sigma=0.5$, $\Delta t=0.00025$, and $\hat{\nu}=1$ at $t=1$ for Example 2

M	Present method				Ref. [19]		Ref. [35]		Ref. [36]	
	L_2	ROC	L_∞	ROC	L_2	L_∞	L_2	L_∞	L_2	L_∞
10	4.610e−04	–	6.430e−04	–	4.353e−04	7.311e−04	1.787e−03	2.416e−03	1.4626e−05	1.9866e−05
20	1.141e−04	2.01	1.588e−04	2.02	1.830e−04	2.733e−04	4.403e−04	5.836e−04	1.3963e−05	1.9805e−05
40	2.844e−05	2.00	3.958e−05	2.00	4.198e−05	6.323e−05	9.273e−05	1.205e−04	1.3799e−05	1.9579e−05
80	7.099e−06	2.00	9.880e−06	2.00	1.982e−06	4.192e−06	6.221e−06	1.616e−05	1.3759e−05	1.9531e−05

Table 9 The comparison of error norms for $\alpha=0.5$, $\sigma=0.5$, $M=80$, and $\hat{\nu}=1$ at $t=1$ for Example 2

Methods	Error norms	$\Delta t=$**0.002**	$\Delta t=$**0.001**	$\Delta t=$**0.0005**
Present	L_2	1.202694e−05	1.039510e−05	8.719828e−06
	L_∞	1.673450e−05	1.445829e−05	1.213331e−05
Ref. [19]	L_2	1.24076e−04	5.4112e−05	1.9282e−05
	L_∞	1.75640e−04	7.7491e−05	2.8460e−05
Ref. [35]	L_2	1.71076e−04	7.0874e−05	2.1092e−05
	L_∞	2.39785e−04	1.00354e−04	3.0679e−05
Ref. [36]	L_2	1.1600e−04	6.1505e−05	3.4177e−05
	L_∞	1.6442e−04	8.7080e−05	4.8293e−05

Table 10 The comparison of error norms with $\sigma=0.5$, $M=80$, $\Delta t=0.00025$, and $\hat{\nu}=1$ at $t=1$ for various values of fractional order α for Example 2

Methods	Error norms	$\alpha=$**0.1**	$\alpha=$**0.25**	$\alpha=$**0.75**	$\alpha=$**0.9**
Present	L_2	1.8876e−05	1.6380e−05	1.3566e−06	4.1799e−07
	L_∞	2.6330e−05	2.2826e−05	1.9250e−06	5.9768e−07
Ref. [19]	L_2	3.492e−06	2.733e−06	1.520e−06	1.886e−06
	L_∞	6.455e−06	5.257e−06	3.443e−06	4.065e−06
Ref. [35]	L_2	1.0027e−05	9.121e−06	2.297e−06	5.283e−06
	L_∞	2.2129e−05	2.0782e−05	8.187e−06	7.886e−06

Example 3 Finally, we consider the TFNB Eq. (1) for

$$f(x,t)=\left(\frac{2t^{2-\alpha}}{\lceil 3-\alpha}+2\pi t^2\left(2\hat{\nu}\pi+t^2\cos(2\pi x)\right)\right)\sin(2\pi x)$$

with $\nu(x,t)=t^2\sin(2\pi x)$.

Finally, Example 3 is approximated for free parameter $\hat{p}=0.5$. Table 11 shows the comparison of present, existing [19], and exact solutions with $\sigma=0.5$, $\alpha=0.5$, $\Delta t=0.00025$, and $\hat{\nu}=1$ for different grid sizes $M=40$ and 80, while Table 12 determines it with $\sigma=0.5$, $\alpha=0.5$, $M=120$, and $\hat{\nu}=1$ at $t=1$ for $\Delta t=0.0025$, 0.002, 0.001, and 0.0005. Figure 7 shows the graphical comparison of exact and approximated solutions with $\sigma=0.5$, $\alpha=0.5$, $\Delta t=0.001$, $\hat{\nu}=1$, and $M=20$ at $t=0.2$, 0.4, 0.6, 0.8, and 1, while Fig. 8 depicts exact and approximate solutions along with absolute errors for $\sigma=0.5$, $\alpha=0.5$, $M=120$, $\Delta t=0.001$, and $\hat{\nu}=1$ at $t=1$.

5 Discussion

Table 2 compares obtained solutions with those solutions presented in [19] for parameters $\sigma=0.5$, $\alpha=0.5$, $\Delta t=0.00025$, and $\hat{\nu}=1$ at $t=1$ for grids $M=10$, 20, 40, and 80. Table 3 compares L_2 and L_∞ errors of the proposed and QBSG methods [19] with $\alpha=0.5$, $\Delta t=0.00025$, and $\hat{\nu}=1$ at $t=1$ for hybrid parameters $\sigma=0.1$, 0.5, and 0.9 and grids $M=10$, 20, 40, and 80. Tables 4 and 5 exhibit the comparison of the proposed method with QBSG method [19] with the parameters $\sigma=0.5$, $\alpha=0.5$, $M=80$, and $\hat{\nu}=1$ at $t=1$ for $\Delta t=0.002$, 0.001, 0.0005, and 0.00025 while Table 6 exhibits the comparison together with convergence rate with $\alpha=0.5$, $\sigma=0.5$, $\Delta t=0.00025$, and $\hat{\nu}=1$ at $t=1$ for grids $M=10$, 20, 40, and 80. Obviously, obtained results are closer than exact solutions, and error norms are better than error norms presented in [19], and the proposed method is second-order accurate in space variable. The L_2 and L_∞ error norms in Table 7 show that solutions

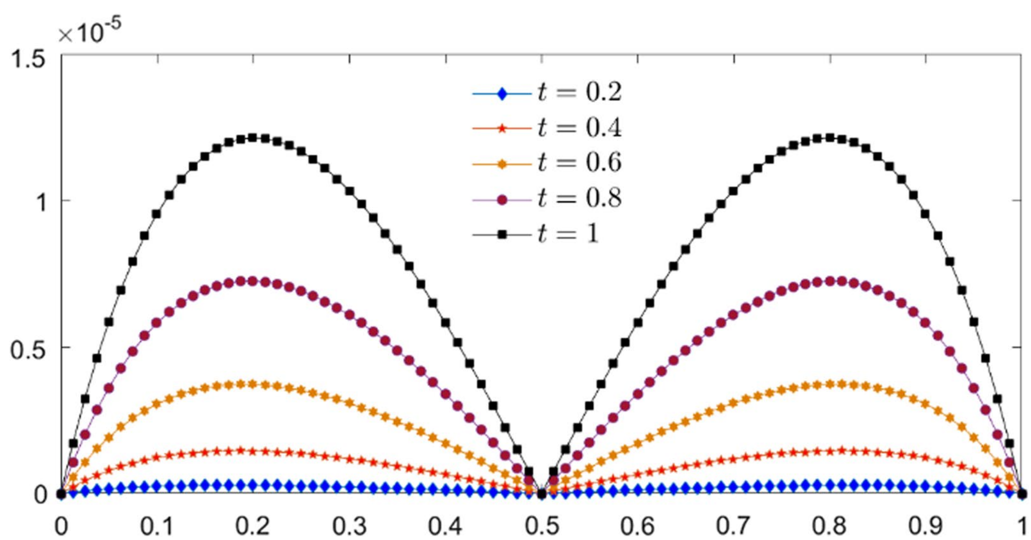

Fig. 4 Absolute error norms for $\alpha=0.5$, $\hat{p}=0.015$, $\sigma=0.5$, $M=80$, $\Delta t=0.0005$, and $\hat{\nu}=1$ for Example 2

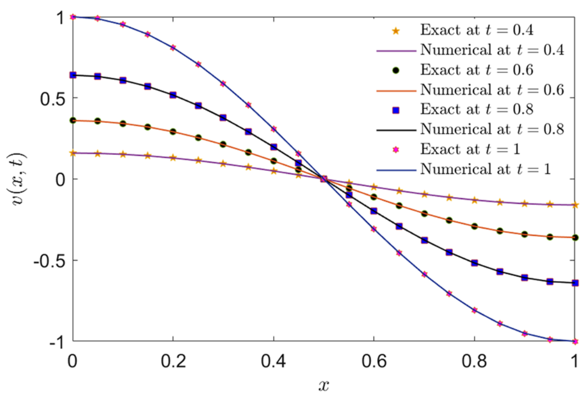

Fig. 5 The comparison of the exact and numerical solutions for $\alpha = 0.5$, $\hat{p}=0.015$, $\sigma=0.5$, $\hat{\nu}=1$, $M=20$, and $\Delta t=0.001$ at various times for Example 2

are more accurate for hybrid parameter 0.9. From Figs. 1–3, an excellent agreement is noticed between exact and approximate solutions with absolute error in ($\approx 10^{-3}$ to 10^{-4}).

Next, Example 2 is solved with free parameter $\hat{p}=0.015$ and $\hat{\nu}=1$ and for various other parameters. The L_2 and L_∞ error norms depicted in Tables 8 and 9 show that the proposed method results are better than those presented in [19, 35, 36], and the proposed method is second-order accurate in space variable. It is also observed that both error norms L_2 and L_∞ are decreasing on increasing the space as well as time mesh sizes. Now, Table 10 shows the error norms for fractional orders $\alpha=0.1$, 0.25, 0.75, and 1. In the case of higher fractional orders, the proposed method results are more accurate than presented in [19, 35]. The small absolute error norms ($\approx 10^{-5}$) shown in Fig. 4 exhibit that solutions are very accurate, while Figs. 5 and 6 show an excellent agreement between exact and approximate solutions.

Finally, Example 3 is solved with free parameter $\hat{p}=0.5$, hybrid parameter $\sigma=0.5$, fractional order $\alpha=0.5$, and $\hat{\nu}=1$ for various space and time meshes at $t=1$. Tables 11 and 12 reveal that the proposed method results are more accurate than the results presented in [19] and are very close to the exact solutions. Figures 7 and 8 compare

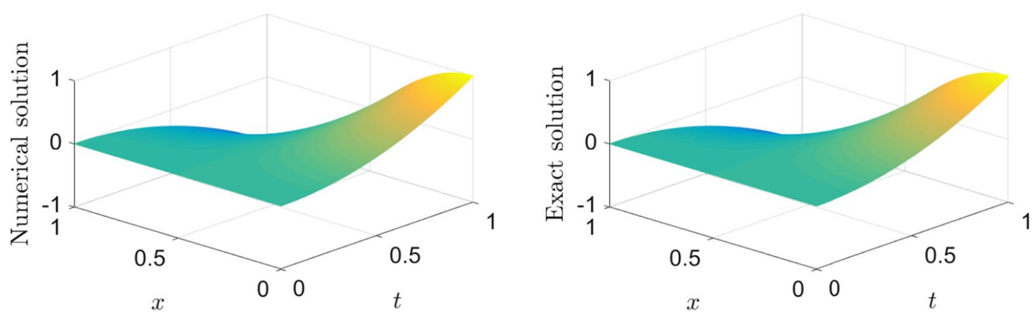

Fig. 6 Surface behavior of the exact and numerical solutions for $\alpha = 0.5$, $\hat{p}=0.015$, $\sigma=0.5$, $M=80$, $\Delta t=0.0005$, and $\hat{\nu}=1$ for Example 2

Table 11 The comparison of present, existing, and exact solutions with $\sigma=0.5$, $\alpha=0.5$, $\Delta t=0.00025$, and $\hat{\nu}=1$ for Example 3

x	Present $M=40$	QBSG [19] $M=40$	Present $M=80$	QBSG [19] $M=80$	Exact
0.0	0.000000	0.000000	0.000000	0.000000	0.000000
0.1	0.587374	0.585106	0.587682	0.587257	0.587785
0.2	0.950372	0.947079	0.950885	0.950262	0.951057
0.3	0.950349	0.947320	0.950879	0.950310	0.951057
0.4	0.587336	0.585586	0.587673	0.587348	0.587785
0.5	0.000000	0.000001	0.000000	0.000000	0.000000
0.6	−0.587336	−0.585584	−0.587673	−0.587346	−0.587785
0.7	−0.950349	−0.947318	−0.950879	−0.950310	−0.951057
0.8	−0.950372	−0.947078	−0.950885	−0.950260	−0.951057
0.9	−0.587374	−0.585106	−0. 0.587682	−0.587257	−0.587785
1.0	0.000000	0.000000	0.000000	0.000000	0.000000
L_2	5.176643e−04	2.899412e−03	1.293988e−04	5.77143e−04	
L_∞	7.313814e−04	4.063808e−03	1.830408e−04	8.13220e−04	

Table 12 The comparison of present, existing, and exact solutions with $\sigma=0.5$, $\alpha=0.5$, $M=120$, and $\hat{\nu}=1$ at $t=1$ for Example 3

	Present	**QBSG [19]**	**Present**	**QBSG [19]**	**Present**	**QBSG [19]**	**Present**	**QBSG [19]**	**Exact**
x	$\Delta t=0.0025$		$\Delta t=0.002$		$\Delta t=0.001$		$\Delta t=0.0005$		
0.0	0.000000	0.000000	0.000000	0.000000	0.000000	0.000000	0.000000	0.000000	0.000000
0.1	0.587705	0.588970	0.587708	0.588675	0.587719	0.588083	0.587729	0.587788	0.587785
0.2	0.950923	0.952952	0.950927	0.952484	0.950945	0.951545	0.950963	0.951076	0.951057
0.3	0.950916	0.952914	0.950922	0.952458	0.950940	0.951544	0.950959	0.951086	0.951057
0.4	0.587695	0.588914	0.587698	0.588635	0.587711	0.588087	0.587723	0.587810	0.587785
0.5	0.000000	0.000005	0.000000	0.000005	0.000000	0.000005	0.000000	0.000004	0.000000
0.6	−0.587695	−0.588905	−0.587698	−0.588630	−0.587711	−0.588077	−0.587723	−0.587801	−0.587785
0.7	−0.950916	−0.952912	−0.950922	−0.952456	−0.950940	−0.951540	−0.950959	−0.951084	−0.951057
0.8	−0.950923	−0.952949	−0.950927	−0.952479	−0.950945	−0.951540	−0.950963	−0.951070	−0.951057
0.9	−0.587705	−0.588968	−0.587708	−0.588672	−0.587719	−0.588080	−0.587729	−0.587784	−0.587785
1.0	0.000000	0.000000	−0.587708	0.000000	0.000000	0.000000	0.000000	0.000000	0.000000
L_2	1.0200e−04	1.39237e−03	9.7988e−05	1.04859e−03	8.4639e−05	3.5948e−04	7.0823e−05	1.7823e−05	
L_∞	1.4438e−04	1.97435e−03	1.3870e−04	1.48780e−03	1.1979e−04	5.1210e−04	1.0022e−04	3.2161e−05	

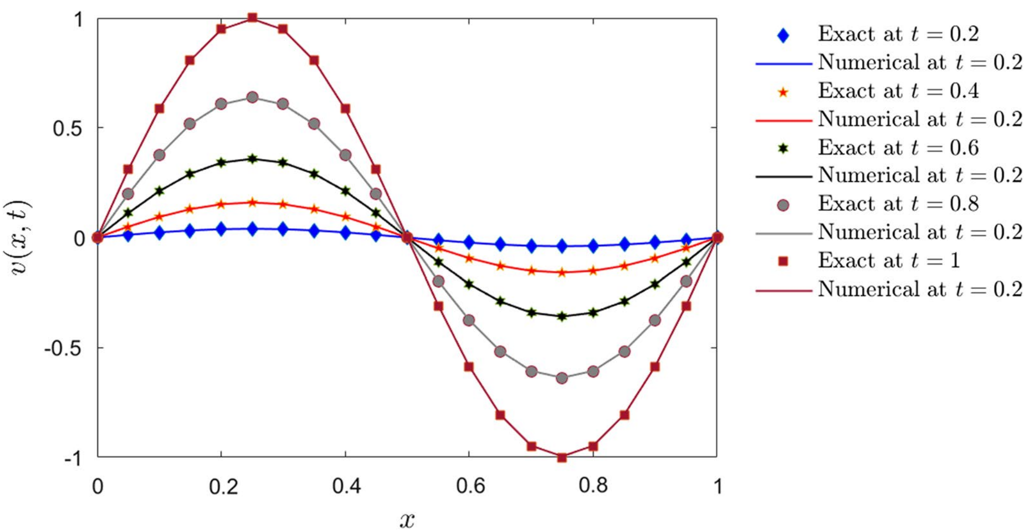

Fig. 7 Comparison of exact and approximated solutions with $\sigma=0.5$, $\alpha=0.5$, $\Delta t=0.001$, $\hat{\nu}=1$, and $M=20$ at $t=0.2$, 0.4, 0.6, 0.8, and 1 for Example 3

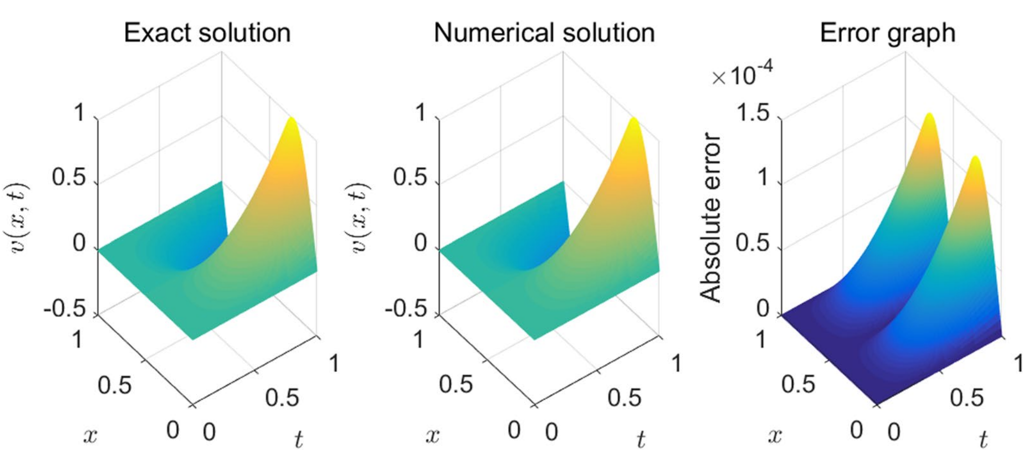

Fig. 8 The exact and approximate solutions, along with abs. errors for $\sigma=0.5$, $\alpha=0.5$, $M=120$, $\Delta t=0.001$, and $\hat{\nu}=1$ at $t=1$ for Example 3

exact and approximated solutions with $\sigma = 0.5$, $\alpha = 0.5$, $\Delta t = 0.001$, $\hat{\nu} = 1$, and $M = 20$ and 120, respectively. An excellent agreement is observed between exact and approximated solutions with absolute error in ($\approx 10^{-4}$).

6 Conclusions

A new cubic HB-spline collocation technique has been established for the numerical treatment of the Caputo TFNB equation. The technique is used for discretizing the spatial derivatives. The Rubin–Graves type quasi-linearization technique has been employed to linearize the nonlinear terms. The three examples have been considered to validate the accuracy and efficiency of the proposed method. It has been observed that the present method provides better results than the methods in [19, 35, 36]. The graphical results are also presented that confirm the accuracy of the proposed algorithm. As we can see, Figs. 2, 3, 6, and 8 are clear representations of the smoothness between numerical and exact solutions, while Figs. 1–3, 4, 7, and 8 expose that absolute errors are very low in ($\approx 10^{-3}$ to 10^{-5}).

Abbreviations

HB-spline	Hybrid B-spline
TFNB	Time fractional nonlinear Burgers'
QBSG	Quadratic B-spline Galerkin
CTBS	Cubic trigonometric B-splines
CPS	Cubic parametric splines
CB-spline	Cubic B-spline

Acknowledgements
Not applicable.

Author contributions
M.T., D.N., and N.D. wrote the original draft, methodology, and investigations, and analyzed the results. A.C. did review and editing of the manuscript. All authors reviewed the manuscript.

Funding
Not available.

Availability of data and materials
Not applicable.

Declarations

Ethics approval and consent to participate
Not applicable.

Consent for publication
Not available.

Competing interests
Authors declare that they have no competing interests.

Received: 29 May 2023 Accepted: 18 October 2023
Published online: 27 October 2023

References

1. Rubin SG, Graves RA (1975) Viscous flow solutions with a cubic spline approximation. Comput Fluids. https://doi.org/10.1016/0045-7930(75)90006-7
2. Zhang W, Cai X, Holm S (2014) Time-fractional heat equations and negative absolute temperatures. Comput Math Appl 67(1):164–171. https://doi.org/10.1016/j.camwa.2013.11.007
3. Tamsir M, Dhiman N, Nigam D, Chauhan A (2021) Approximation of caputo time-fractional diffusion equation using redefined cubic exponential B-spline collocation technique. AIMS Math. https://doi.org/10.3934/math.2021226
4. Shukla HS, Tamsir M, Srivastava VK, Rashidi MM (2016) Modified cubic B-spline differential quadrature method for numerical solution of three dimensional coupled viscous Burger equation. Mod Phys Lett B 30(11):1650110
5. Roul P, Goura VP (2021) A high-order B-spline collocation scheme for solving a nonhomogeneous time-fractional diffusion equation. Math Methods Appl Sci 44(1):546–567. https://doi.org/10.1002/mma.6760
6. Diethelm K, Ford NJ, Freed AD (2002) A predictor-corrector approach for the numerical solution of fractional differential equations. Nonlinear Dyn 29(1–4):3–22. https://doi.org/10.1023/A:1016592219341
7. Rihan FA, Baleanu D, Lakshmanan S, Rakkiyappan R (2014) On fractional SIRC model with salmonella bacterial infection. Abstr Appl Anal. https://doi.org/10.1155/2014/136263
8. Debnath L (2003) Recent applications of fractional calculus to science and engineering. Int J Math Math Sci 54:3413–3442. https://doi.org/10.1155/S0161171203301486
9. Shafiq M, Abbas M, Abdullah FA, Majeed A, Abdeljawad Th, Alqudah MA (2022) Numerical solutions of time fractional Burgers' equation involving Atangana-Baleanu derivative via cubic B-spline functions. Results Phys 34:105244
10. Liao W (2008) An implicit fourth-order compact finite difference scheme for one-dimensional Burgers' equation. Appl Math Comput 206(2):755–764. https://doi.org/10.1016/J.AMC.2008.09.037
11. Liu X, Fang H (2019) Periodic pulse control of Hopf bifurcation in a fractional-order delay predator–prey model incorporating a prey refuge. Adv Differ Equ. https://doi.org/10.1186/s13662-019-2413-9
12. Taufiq M, Uddin M (2021) Numerical solution of fractional order anomalous subdiffusion problems using radial kernels and transform. J Math. https://doi.org/10.1155/2021/9965734
13. Majeed A, Kamran M, Iqbal MK, Baleanu D (2020) Solving time fractional Burgers' and Fisher's equations using cubic B-spline approximation method". Adv Differ Equ 1:1–15. https://doi.org/10.1186/S13662-020-02619-8/TABLES/8
14. Kashif M, Dwivedi KD, Som T (2022) Numerical solution of coupled type Fractional order Burgers' equation using finite difference and fibonacci collocation method. Chin J Phys 77:2314–2323. https://doi.org/10.1016/J.CJPH.2021.10.044
15. Zeng F, Zhang Z, Karniadakis GE (2015) A generalized spectral collocation method with tunable accuracy for variable-order fractional differential equations. SIAM J Sci Comput 37(6):A2710–A2732. https://doi.org/10.1137/141001299
16. Khader MM, Saad KM, Hammouch Z, Baleanu D (2021) A spectral collocation method for solving fractional KdV and KdV-Burgers equations with non-singular kernel derivatives. Appl Numer Math 161:137–146. https://doi.org/10.1016/J.APNUM.2020.10.024
17. Taghipour M, Aminikhah H (2022) Application of Pell collocation method for solving the general form of time-fractional Burgers equations. Math Sci 2022:1–19. https://doi.org/10.1007/S40096-021-00452-Y
18. Zhao T, Wu Y (2021) Hermite cubic spline collocation method for nonlinear fractional differential equations with variable-order. Symmetry 13(5):872. https://doi.org/10.3390/SYM13050872
19. Esen A, Tasbozan O (2015) Numerical solution of time fractional Burgers equation. Acta Univ Sapientiae Math 7(2):167–185. https://doi.org/10.1515/ausm-2015-0011
20. Liu F, Zhuang P, Anh V, Turner I, Burrage K (2007) Stability and convergence of the difference methods for the space-time fractional advection-diffusion equation. Appl Math Comput 191(1):12–20. https://doi.org/10.1016/j.amc.2006.08.162
21. Huang Y, Zadeh FM, Skandari MHN, Tehrani HA, Tohidi E (2020) Space-time Chebyshev spectral collocation method for nonlinear

time-fractional Burgers equations based on efficient basis functions. Math Methods Appl Sci 44(5):4117–4136. https://doi.org/10.1002/MMA.7015
22. Yaseen M, Abbas M (2020) An efficient computational technique based on cubic trigonometric B-splines for time fractional Burgers' equation. Int J Comput Math 97(3):725–738. https://doi.org/10.1080/00207160.2019.1612053
23. El-Danaf TS, Hadhoud AR (2012) Parametric spline functions for the solution of the one time fractional Burgers' equation. Appl Math Model 36(10):4557–4564. https://doi.org/10.1016/j.apm.2011.11.035
24. Ahmed HF, Bahgat MSM, Zaki M (2020) "Numerical study of multidimensional fractional time and space coupled Burgers' equations. Pramana J Phys. https://doi.org/10.1007/s12043-020-1928-7
25. Zhang J, Wei Z, Yong L, Xiao Y (2018) Analytical solution for the time fractional BBM-burger equation by using modified residual power series method. Complexity. https://doi.org/10.1155/2018/2891373
26. Malyk I, Shrahili MMA, Shafay AR, Goswami P, Sharma S, Dubey RS (2020) Analytical solution of non-linear fractional Burger's equation in the framework of different fractional derivative operators. Results Phys 19:103397. https://doi.org/10.1016/J.RINP.2020.103397
27. Syam MI, Obayda DA, Alshamsi W, Al-Wahashi N, Alshehhi M (2019) Generalized solutions of the fractional Burger's equation. Results Phys 15:102525. https://doi.org/10.1016/J.RINP.2019.102525
28. Sripacharasakullert P, Sawangtong W, Sawangtong P (2019) An approximate analytical solution of the fractional multi-dimensional Burgers equation by the homotopy perturbation method. Adv Differ Equ 1:1–12. https://doi.org/10.1186/S13662-019-2197-Y/METRICS
29. Zhuang P, Liu F (2006) Implicit difference approximation for the time fractional diffusion equation. J Appl Math Comput 22(3):87–99
30. Esen A, Ucar Y, Yagmurlu N, Tasbozan O (2013) A Galerkin finite element method to solve fractional diffusion and fractional diffusion-wave equations. Math Model Anal 18:260–273
31. Shukla HS, Tamsir M (2016) Numerical solution of nonlinear sine Gordon equation by using the modified cubic B-spline differential quadrature method. Beni-Suef Univ J Basic Appl Sci 7(4):359–366
32. Padder A, Almutairi L, Qureshi S, Soomro A, Afroz A, Hincal E, Tassaddiq A (2023) Dynamical analysis of generalized tumor model with caputo fractional-order derivative. Fractal Fract 7(3):258. https://doi.org/10.3390/fractalfract7030258
33. Tamsir M, Srivastava VK, Jiwari R (2016) An algorithm based on exponential modified cubic B-spline differential quadrature method for nonlinear Burgers' equation. Appl Math Comput 290:111–124
34. Shukla HS, Tamsir M (2018) An exponential cubic B-spline algorithm for multi-dimensional convection-diffusion equations. Alex Eng J 57(3):1999–2006
35. Esen A, Tasbozan O (2015) Numerical solution of time fractional burgers equation by cubic B-spline finite elements. Mediterr J Math 13(3):1325–1337
36. Singh BK, Gupta M (2022) Trigonometric tension B-spline collocation approximations for time fractional Burgers' equation. J Ocean Eng Sci. https://doi.org/10.1016/j.joes.2022.03.023
37. Shaikh AA, Qureshi S (2022) Comparative analysis of Riemann-Liouville, Caputo-Fabrizio, and Atangana-Baleanu integrals. J Appl Math Comput Mech 21(1):91–101
38. Qureshi S, Akanbi MA, Shaikh AA, Wusu AS, Ogunlaran OM, Mahmoud W, Osman MS (2023) A new adaptive nonlinear numerical method for singular and stiff differential problems. Alex Eng J 74:585–597
39. Roul P (2020) A high accuracy numerical method and its convergence for time-fractional Black-Scholes equation governing European options. Appl Numer Math 151:472–493
40. Strikwerda JC (2004) Finite difference schemes and partial differential equations, 2nd edn. SIAM

Publisher's Note

Springer Nature remains neutral with regard to jurisdictional claims in published maps and institutional affiliations.